# Sparsity-based moving target localization using multiple dual-frequency radars under phase errors

Khodour Al Kadry, Fauzia Ahmad*, and Moeness G. Amin

Radar Imaging Lab, Center for Advanced Communications, Villanova University, Villanova, PA 19085, USA.

## ABSTRACT

In this paper, we consider moving target localization in urban environments using a multiplicity of dual-frequency radars. Dual-frequency radars offer the benefit of reduced complexity and fast computation time, thereby permitting real-time indoor target localization and tracking. The multiple radar units are deployed in a distributed system configuration, which provides robustness against target obscuration. We develop the dual-frequency signal model for the distributed radar system under phase errors and employ a joint sparse scene reconstruction and phase error correction technique to provide accurate target location and velocity estimates. Simulation results are provided that validate the performance of the proposed scheme under both full and reduced data volumes.

**Keywords:** Dual frequency radar, position velocity estimation, compressive sensing, through-the-wall radar.

## 1. INTRODUCTION

Detection and localization of moving targets are highly desirable in urban sensing applications, such as surveillance and reconnaissance, searching for survivors in natural disasters, and hostage rescue missions.[1] The recent trend in ground-based urban radar system technology is the use of distributed configurations of man-portable radar units, which provide an effective and flexible alternative to vehicle-mounted large-aperture systems for localizing moving targets in urban environments. The individual radar units can be either wideband radars, such as linear frequency modulated or pulse-Doppler radars[2], or dual-frequency radars.[3,4] In particular, dual-frequency technology provides a viable solution to address the operational constraints on cost and system complexity for moving target localization in urban sensing applications.[5-7]

In this paper, we consider a network of dual-frequency radars for moving target localization and velocity estimation in urban environments using sparsity-based techniques. The radar units are deployed in a distributed configuration around a sparse scene of a few moving targets. This allows the radar units to view the targets from different aspect angles. The Doppler velocity diversity provided by the distributed configuration enables estimation of the horizontal and vertical target velocity components. The baseband returns measured at each radar unit are communicated to a central processing station, where they are combined using sparsity-based techniques to estimate both target position and velocity. However, in practical operational scenarios, the radar unit locations and/or wall parameters may not be known accurately. Such inaccuracies typically manifest themselves as phase errors in the baseband radar measurements, which if unaccounted for, may lead to degraded system performance. We propose a sparsity-driven approach for joint position-velocity estimation and phase error correction, which introduces a diagonal matrix to model the phase errors and iterates between sparse signal recovery and phase error estimation steps.

The remainder of the paper is organized as follows. Section 2 describes the dual-frequency signal model under phase errors, while the joint position-velocity estimation and phase error correction approach is detailed in Section 3. Supporting simulation results are provided in Section 4, followed by concluding remarks in Section 5.

*fauzia.ahmad@villanova.edu; http://www1.villanova.edu/villanova/engineering/research/centers/cac/facilities/rillab.html

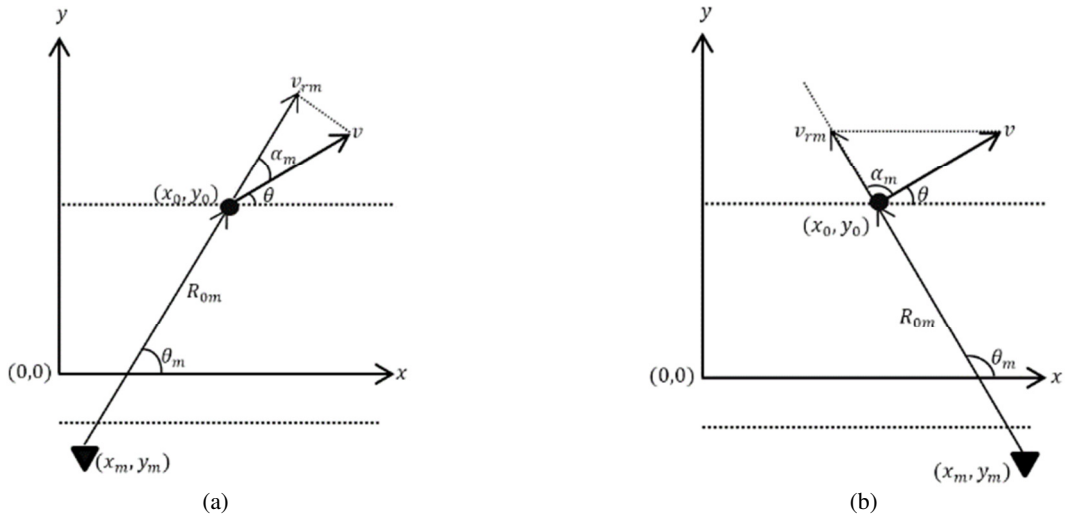


Figure 1: Free space scene geometry, (a) first case, (b) second case.

## 2. SIGNAL MODEL

Assume that $M$ dual-frequency radar units, each operating at frequencies $f_1$ and $f_2$, are distributed around the region of interest in the $(x, y)$-plane. The measurements from all radar units are communicated to a central processing station where they are combined to reconstruct the scene being interrogated. Since the targets' aspect angles may vary widely across the radar units in the distributed configurations, only a noncoherent combination of the measurements from the $M$ radar units is possible. Below, we first describe the signal model for a single dual-frequency radar unit and then extend it to multiple radar units.

### 2.1 Single Radar Unit

Let the $m$th radar unit location be given by the position vector $\boldsymbol{x}_m = (x_m, y_m)$. Assume that a single target is present at initial position $\boldsymbol{x}_0 = (x_0, y_0)$, moving with uniform velocity $v$ in the direction $\theta$, as shown in Fig. 1. Let $v_x = v\cos(\theta)$ and $v_y = v\sin(\theta)$ denote the horizontal and vertical target velocity components, respectively. The target is assumed to be undergoing linear motion, with the range-to-motion given by

$$R_m(t) = R_{0m} + v_{rm}t, \tag{1}$$

where $R_{0m}$ is the initial target range and is given by

$$R_{0m} = \sqrt{(x_0 - x_m)^2 + (y_0 - y_m)^2}, \tag{2}$$

and $v_{rm}$ is the target radial velocity and is expressed as

$$v_{rm} = v\cos(\alpha_m) \tag{3}$$

In (3), $\alpha_m$ is the angle between the direction of target motion and the radar line-of-sight (LOS) (see Fig. 1), given by

$$\alpha_m = \theta_m - \theta \tag{4}$$

where $\theta_m$ is the angle between the radar LOS and the $x$-axis. For the case depicted in Fig .1(a), $\theta_m$is given by

$$\theta_m = \tan^{-1}\left(\frac{y_m - y_0}{x_m - x_0}\right), \tag{5}$$

whereas that corresponding to Fig. 1(b) is expressed as

$$\theta_m = \pi - \tan^{-1}\left(\frac{y_m - y_0}{x_m - x_0}\right). \tag{6}$$

The baseband radar return, corresponding to the $i$th frequency, is expressed as

$$s_{im}(t) = \rho_m \exp\left(-j\frac{4\pi f_i}{c}(R_{0m} + v_{rm}t) + \alpha_{im}\right), i = 1, 2 \tag{7}$$

where $\rho_m$is the amplitude of the return, which is assumed to be frequency-independent, $c$ is the speed of propagation in free-space, and $\alpha_{im}$ is the phase error corresponding to the $i$th frequency at the $m$th radar unit. For the case of $K$ moving targets, the radar return is the superposition of the individual target returns, i.e.,

$$s_{im}(t) = \sum_{k=0}^{K-1} \rho_{km} \exp\left(-j\frac{4\pi f_i}{c}\left(R_{0,km} + v_{r,km}t\right) + \alpha_{im}\right), i = 1, 2. \tag{8}$$

Substituting (2)-(4) in (8), we obtain

$$s_{im}(t) = \sum_{k=0}^{K-1} \rho_{km} \exp\left(-j\frac{4\pi f_i}{c}\left(\sqrt{\left(x_{0,k} - x_m\right)^2 + \left(y_{0,k} - y_m\right)^2} + (v_{x,k}\cos\theta_{km} + v_{y,k}\sin\theta_{km})t\right) + \alpha_{im}\right). \tag{9}$$

Assume that the region of interest is divided into $N_x \times N_y$ pixels in the crossrange $(x)$ and downrange $(y)$. Likewise, the horizontal and vertical velocity components are sampled on a discrete grid of $N_{vx} \times N_{vy}$ values. In other words, an image with $N_x \times N_y$ pixels is associated with each considered horizontal and vertical velocity pair, resulting in a four dimensional (4D) target space. Let $\boldsymbol{r}^{(m)}$ denote the target state vector for the $m$th radar unit. If a target exists at a specific point in the 4D space, the corresponding element of $\boldsymbol{r}^{(m)}$ assumes a non-zero value; otherwise, it is zero. Sampling the baseband radar return $s_{im}(t)$ at times $\{t_n\}_{n=0}^{N-1}$ and appending $N$ samples at each of the two frequencies $f_1$ and $f_2$, we form a $2N \times 1$ measurement vector $\boldsymbol{s}^{(m)}$ corresponding to the $m$th radar unit, which using (9) can be expressed in matrix-vector form as

$$\boldsymbol{s}^{(m)} = \boldsymbol{\alpha}^{(m)}\boldsymbol{\Psi}^{(m)}\boldsymbol{r}^{(m)}, m = 1,2, \ldots, M \tag{10}$$

where

$$\boldsymbol{\Psi}^{(m)} = \left[\left(\boldsymbol{\Psi}_1^{(m)}\right)^T \quad \left(\boldsymbol{\Psi}_2^{(m)}\right)^T\right]^T \tag{11}$$

is of dimension $2N \times N_x N_y N_{vx} N_{vy}$ with the $(n, q)$th element of $\boldsymbol{\Psi}_{\boldsymbol{i}}^{(m)}, i = 1,2$, given by

$$\left[\boldsymbol{\Psi}_{\boldsymbol{i}}^{(m)}\right]_{n,q} = \exp\left(-j\frac{4\pi f_i}{c}\left(\sqrt{\left(x_{0,q} - x_m\right)^2 + \left(y_{0,q} - y_m\right)^2} + (v_{x,q}\cos\theta_{qm} + v_{y,q}\sin\theta_{qm})n\right)\right), \tag{12}$$

$$\boldsymbol{\alpha}^{(m)} = \text{blkdiag}(\boldsymbol{\alpha}_{1m}, \boldsymbol{\alpha}_{2m}),\ \boldsymbol{\alpha}_{im} = \exp(-j\alpha_{im})\,\boldsymbol{I}, \tag{13}$$

and $\boldsymbol{I}$ is an $N \times N$ identity matrix.

### 2.2 Multiple Radar Units

Stacking the measurement vectors corresponding to all $M$ radar units results in a $2MN \times 1$ measurement vector

$$\mathbf{s} = \left[\left(\boldsymbol{s}^{(1)}\right)^T \quad \cdots \quad \left(\boldsymbol{s}^{(M)}\right)^T\right]^T. \tag{14}$$

Concatenating the phase error and dictionary matrices to form a composite phase error matrix $\boldsymbol{\alpha} \in \mathbb{C}^{2MN \times 2MN}$and a composite dictionary matrix $\boldsymbol{\Psi} \in \mathbb{C}^{2MN \times MN_x N_y N_{v_x} N_{v_y}}$ as

$$\boldsymbol{\alpha} = \text{blkdiag}\left(\boldsymbol{\alpha}^{(1)}, \boldsymbol{\alpha}^{(2)}, \dots, \boldsymbol{\alpha}^{(M)}\right), \quad \boldsymbol{\Psi} = \text{blkdiag}\left(\boldsymbol{\Psi}^{(1)}, \boldsymbol{\Psi}^{(2)}, \dots, \boldsymbol{\Psi}^{(M)}\right), \tag{15}$$

we obtain the linear model

$$\boldsymbol{s} = \boldsymbol{\alpha}\boldsymbol{\Psi}\mathbf{r} \tag{16}$$

where

$$\boldsymbol{r} = \left[\left(\boldsymbol{r}^{(1)}\right)^T \quad \dots \quad \left(\boldsymbol{r}^{(M)}\right)^T\right]^T. \tag{17}$$

Note that the vector $\boldsymbol{r}$ exhibits a group sparse structure, since the target state vectors, $\boldsymbol{r}^{(m)}, m = 1,2, \dots, M$, describe the same 4D target space. That is, the vectors $\boldsymbol{r}^{(1)} \dots, \boldsymbol{r}^{(M)}$ share a common sparsity pattern.

Note that for the case where some of the time samples at each frequency are unavailable due to intentional or unintentional interference and/or impulsive noise, the model in (16) can be modified by introduction of a $2MN_A \times 2MN \ \ (N_A < N)$ measurement matrix $\boldsymbol{\Phi}$ as

$$\bar{\boldsymbol{s}} = \boldsymbol{\Phi}\boldsymbol{\alpha}\boldsymbol{\Psi}\boldsymbol{r} \tag{18}$$

The measurement matrix can be of different types, as reported in Refs. [8]-[9].

## 3. JOINT SCENE RECOVERY AND PHASE ERROR CORRECTION

In this section, we focus on the full measurement model of (16). Note that the reconstruction scheme described below is also applicable to the reduced measurement model of (18).

If conventional group sparse reconstruction techniques, such as simultaneous orthogonal matching pursuit (SOMP)[10] or Group Lasso,[11] are used to recover the vector $\boldsymbol{r}$ in the presence of phase errors, the resulting target position and velocity estimates will be biased. Instead, alternate methods involving a non-quadratic regularization for joint position-velocity estimation and phase error correction can be applied.[12] More specifically, the problem can be posed as the minimization of the cost function

$$J(\mathbf{r}, \boldsymbol{\alpha}) = \ \|\boldsymbol{s} - \boldsymbol{\alpha}\boldsymbol{\Psi}\mathbf{r}\|_2^2 + \lambda\|\mathbf{r}\|_{1,2}, \tag{19}$$

where $\lambda$ is the regularization parameter and $\|\cdot\|_{1,2}$ denotes the mixed $l_1/l_2$ norm promoting group sparsity.[13] The cost function in (19) is minimized jointly with respect to $\mathbf{r}$ and $\boldsymbol{\alpha}$ using a block coordinate descent technique.[14] The algorithm is an iterative algorithm, which cycles through steps of position-velocity estimation and phase error estimation. That is, each iteration involves two steps: i) The cost function is minimized with respect to the scene, and ii) The phase error is estimated given the scene estimate. Before moving on to the next iteration, the signal model is updated using the estimated phase error. This flow is outlined in Table 1, where $p$ denotes the iteration number and $\hat{\mathbf{r}}^{(p)}$ and $\widehat{\boldsymbol{\alpha}}^{(p)}$ are the scene and the phase error estimates at iteration $p$, respectively. Note that the phase error corrupted data $\boldsymbol{s}$ and the dictionary $\boldsymbol{\Psi}$ are known quantities. The unknowns are the scene $\mathbf{r}$ and the phase error $\boldsymbol{\alpha}$.

Table 1. Flow of the joint optimization method.

Initialize $p = 0$, $\boldsymbol{\alpha}^{(0)} = \boldsymbol{I}$, and $\boldsymbol{\Omega}^{(0)} = \boldsymbol{\alpha}^{(0)}\boldsymbol{\Psi} = \boldsymbol{\Psi}$

1. $\hat{\mathbf{r}}^{(p+1)} = \arg\min_{\mathbf{r}} J\left(\boldsymbol{r}, \ \widehat{\boldsymbol{\alpha}}^{(p)}\right)$
2. $\widehat{\boldsymbol{\alpha}}^{(p+1)} = \arg\ \min_{\boldsymbol{\alpha}} J(\hat{\mathbf{r}}^{(p+1)}, \boldsymbol{\alpha})$
3. $\boldsymbol{\Omega}^{(p+1)} = \widehat{\boldsymbol{\alpha}}^{(p+1)}\ \boldsymbol{\Psi}$
4. If $\frac{\left\|\hat{\mathbf{r}}^{(p+1)} - \hat{\mathbf{r}}^{(p)}\right\|_2^2}{\left\|\hat{\mathbf{r}}^{(p)}\right\|_2^2}$ is less than a predetermined threshold, stop. Otherwise, let $p = p + 1$ and return to step 1.

## 4. SIMULATION RESULTS

Consider three dual-frequency radar units located, respectively, at (-1.2 m, 3 m), (2 m, -1.2 m), and (5.1 m, 4.2 m) in the $(x, y)$-plane. Each radar units uses the following carrier frequencies: 990 MHz and 1 GHz, leading to an unambiguous range of 15 m. Two point moving targets are considered. The first target is at an initial position (3 m, 2 m) and moving with velocities (0 m/s, -0.3 m/s), while the second target is initially located at (1.5 m, 1 m) and moving with velocities (0.5 m/s, 0 m/s). White Gaussian noise is added to the baseband radar returns corresponding to the two carrier frequencies at 10 dB signal-to-noise ratio (SNR). A total of 40 time samples are collected at 10 Hz sampling rate for each radar return.

The region of interest is of dimensions 5 m × 5 m in crossrange and downrange and is discretized on a square grid with a step size of 0.1 m. The horizontal and vertical velocity components ranging between -1 m/s and 1 m/s are considered and sampled with a grid size of 0.1 m/s each. Fig. 2 shows the joint position-velocity estimates of the two moving targets with noisy data using SOMP in the absence of phase errors. Clearly, SOMP provides accurate estimates of position and velocity components. For the case of missing data, we randomly measure 10 samples at each of the two carrier frequencies, thereby retaining only 25% of the data volume. Fig. 4 depicts the joint position-velocity estimates of the two moving targets with noisy missing data using SOMP. Similar to the full data case, we observe that SOMP provides accurate estimates of position and velocity components in the absence of phase errors.

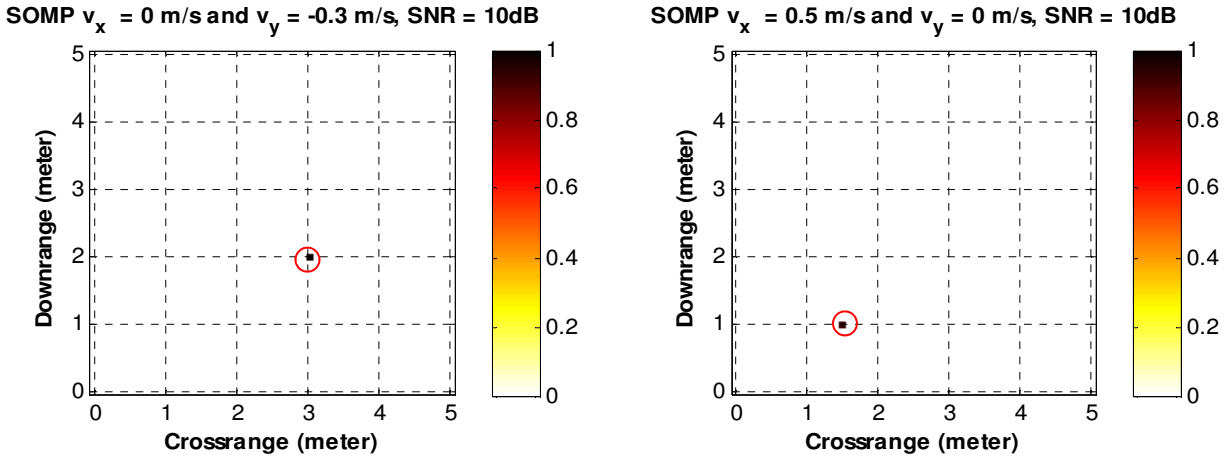


Figure 2: Position-velocity estimates of two moving targets using SOMP in the absence of phase errors under full data volume.

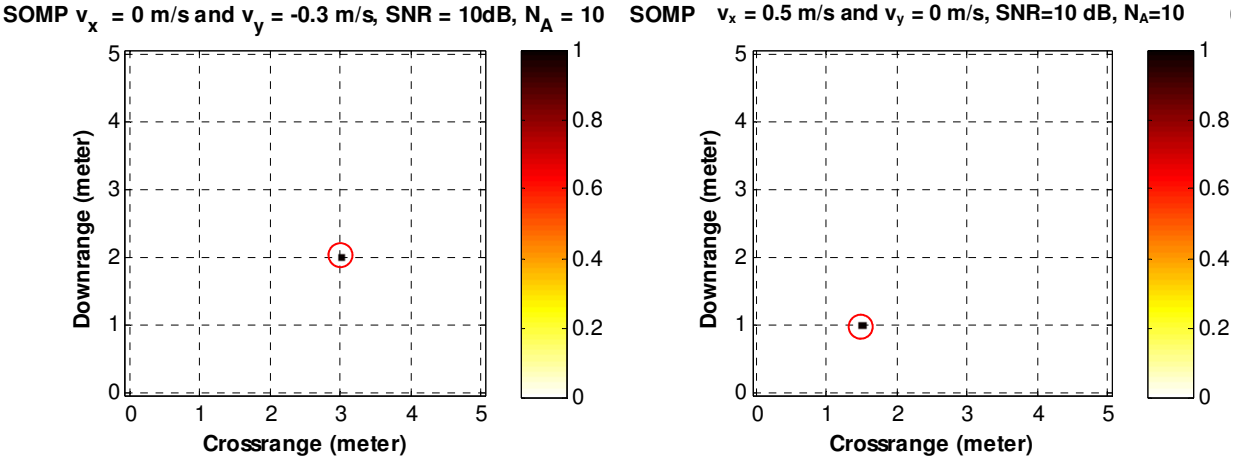


Figure 3: Position-velocity estimates of two moving targets using SOMP in the absence of phase errors under reduced data volume.

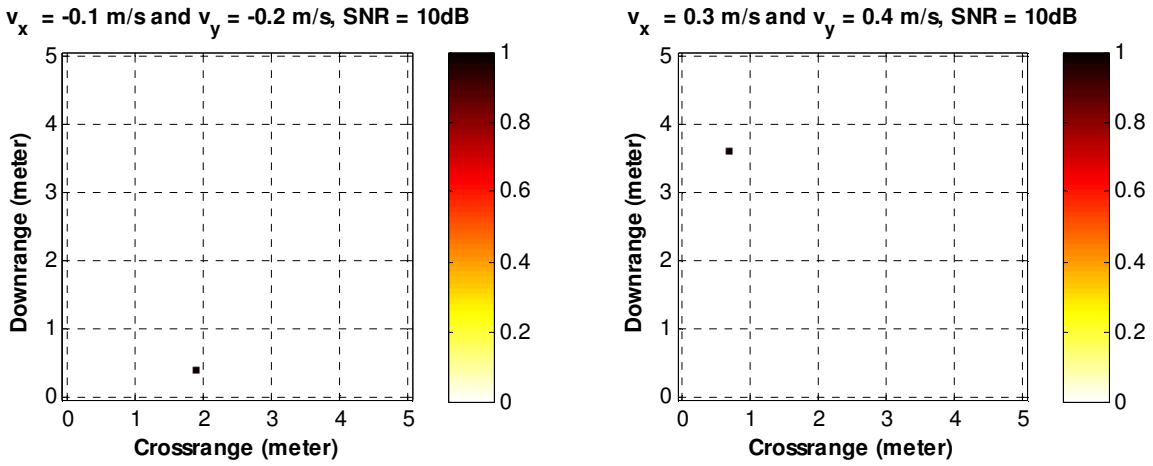


Figure 4: Position-velocity estimates of two moving targets with phase errors using SOMP under full data volume.

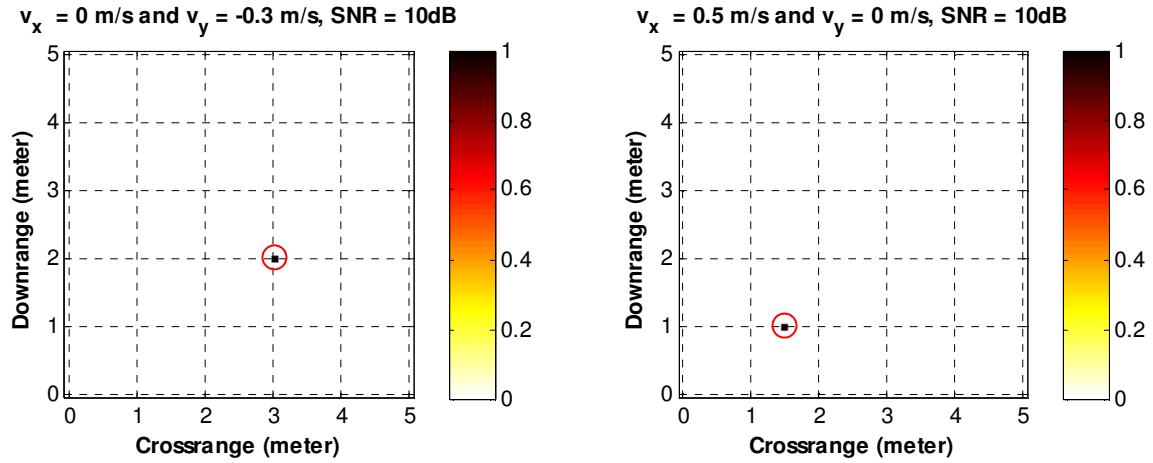


Figure 5: Position-velocity estimates of two moving targets using the proposed method under reduced data volume.

Next, we introduce phase errors in the radar measurements. The phase error at each radar unit at each carrier frequency is assumed to be a uniformly distributed random variable between 0 and $2\pi$. Fig. 4 shows the estimated position and velocity using SOMP with full data and without accounting for the phase errors. Clearly, the estimates are inaccurate, with the estimated position being (1.9 m, 0.4 m) and (0.8 m, 3.6 m), and the estimated velocity being (-0.1 m/s, -0.2 m/s) and (0.3 m/s, 0.4 m/s). Fig. 5 depicts the position-velocity estimates using the joint optimization approach under full data volume. We observe that the proposed technique corrects for the phase errors and provides accurate position and velocity estimates of (1.5 m, 1 m) and (0.5 m/s, 0 m/s) for the first target, and (3 m, 2 m) and (0 m/s, -0.3 m/s) for the second target.

For the case of missing samples under phase errors, we achieve data reduction by randomly selecting 10 samples out of the 40 available samples at each of the two carrier frequencies for each radar unit, thereby retaining 25% of the data volume. Fig. 6 shows the sparse reconstruction estimates of the two moving targets using SOMP without accounting for the phase errors. The estimates are clearly biased with the estimated positions being (4.4 m, 3.6 m), (1.7 m, 1 m), and the velocity estimates are (0.1 m/s, -0.4 m/s) and (0.5 m/s, 0 m/s). Fig. 7 depicts the position-velocity estimates using the joint optimization approach, which provides accurate position and velocity estimates of (1.5 m, 1 m), (0.5 m/s, 0 m/s) for the first target, and (3 m, 2 m) and (0 m/s, -0.3 m/s) for the second target.

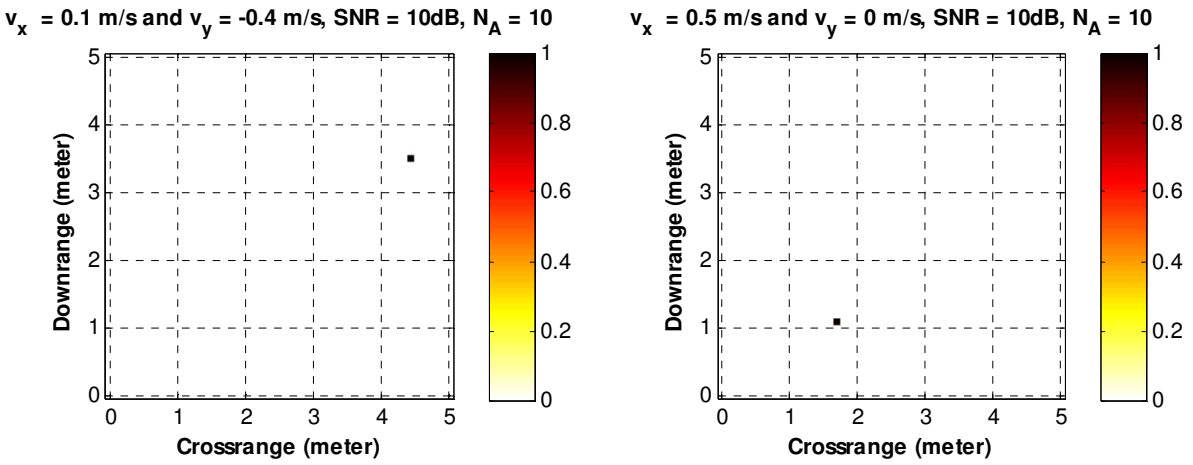


Figure 6: Position-velocity estimates of two moving targets with phase errors using SOMP under reduced data volume.

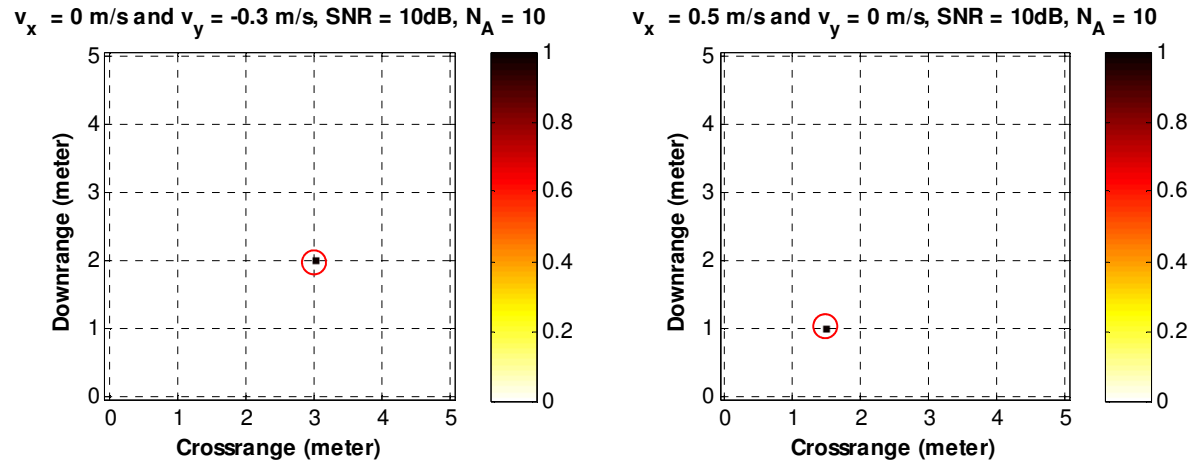


Figure 7: Position-velocity estimates of two moving targets using the proposed method under reduced data volume.

## 5. CONCLUSION

In this paper, we presented a joint sparse scene reconstruction and phase error correction technique to provide target position and motion parameter estimation using a distributed network of dual-frequency radars in urban sensing applications. The phase errors can arise due to uncertainties in radar locations and/or wall parameter ambiguities. The diversity provided by the distributed configuration allows not only the target to be localized in crossrange and downrange, but also enables estimation of the horizontal and vertical target velocity components. Supporting simulation results were provided, which validated the performance of the proposed approach under both full and reduced data volumes.

## ACKNOWLEDGMENT

This work was supported by US Army Research Office/Army Research Lab under contract W911NF-11-1-0536.

## REFERENCES

[1] Amin, M.G. (Ed.), [Through-the-Wall Radar Imaging], CRC Press, Boca Raton, FL, (2011).

[2] Skolnik, M.L., [Introduction to Radar Systems, 3rd Edition], McGraw-Hill, New York, NY, (2001).
[3] Ridenour, L.N., [Radar System Engineering, vol. 1 of MIT Radiation Laboratory Series], McGraw-Hill, NY, (1947).
[4] Boyer, W.D., "A diplex, Doppler, phase comparison radar," IEEE Trans. Aerosp. Navig. Electron., ANE-10(3), 27-33 (1963).
[5] Ahmad, F., Amin, M.G. and Zemany, P.D., "Dual-frequency radars for target localization in urban sensing," IEEE Trans. Aerosp. Electronic Syst., 45(4), 1598-1609 (2009).
[6] Lin, A. and Ling, H., "Location tracking of indoor movers using a two-frequency Doppler and direction-of-arrival (DDOA) radar," Digest IEEE Int. Symp. Antennas Propag., Albuquerque, NM, 1125 – 1128 (2006).
[7] Zhang, Y., Amin, M. G. and Ahmad, F., "A Novel Approach for Multiple Moving Target Localization using Dual-Frequency Radars and Time-Frequency Distributions," Proc. 41th Annual Asilomar Conf. Signals, Systems, and Computers, 1817-1821 (2007).
[8] Gurbuz, A., McClellan, J., and Scott Jr., W., "Compressive sensing for subsurface imaging using ground penetrating radar," Signal Process., 89(10), 1959 - 1972 (2009).
[9] Qian, J., Ahmad, F., and Amin, M.G., "Joint localization of stationary and moving targets behind walls using sparse scene recovery," J. Electronic Imag. 22(2), 021002 (2013).
[10] Yuan, M. and Lin, Y., "Model Selection and Estimation in Regression with Grouped variables", J. royal Stat. Soc., Series B, 68 (1), 49-67 (2007).
[11] Tropp, J.A., Gilbert, A.C., and Strauss, M.J., "Algorithms for Simultaneous Sparse Reconstruction. Part I: Greedy pursuit" Signal Process. 86 (3), 572 – 588 (2006).
[12] Onhon, N. and Cetin, M., "Nonquadratic Regularization-based Technique for Joint SAR Imaging and Model Error Correction," Proc. SPIE, Algorithms for Synthetic Aperture Radar Imagery XVI, 7337, 73370C (2009).
[13] Bach, F., Jenatton, R., Mairal, J., and Obozinski, G., "Convex optimization with sparsity-inducing norms," in S. Sra, S. Nowozin, and S. J. Wright (Eds.), Optimization for Machine Learning, MIT Press, 2011.
[14] Tseng, P. and Yun, S., "A coordinate gradient descent method for nonsmooth separable minimization," Mathematical Programming, 117(1), 387-423 (2009).